Two Antagonistic Hippo Signaling Circuits Set the Division Plane at the Medial Position in the Ciliate *Tetrahymena*

Yu-Yang Jiang,*,[1] Wolfgang Maier,†,[1] Ralf Baumeister,† Ewa Joachimiak,‡ Zheng Ruan,§ Natarajan Kannan,§, Diamond Clarke,* Panagiota Louka,* Mayukh Guha,* Joseph Frankel,†† and Jacek Gaertig*,[2]**

*Department of Cellular Biology, §Institute of Bioinformatics, and **Department of Biochemistry and Molecular Biology, University of Georgia, Athens, Georgia 30602, †Bio 3/Bioinformatics and Molecular Genetics, Faculty of Biology and ZBMZ, Faculty of Medicine, Albert-Ludwigs-University of Freiburg, 79104 Germany, ‡Laboratory of Cytoskeleton and Cilia Biology, Nencki Institute of Experimental Biology of Polish Academy of Sciences, Warsaw 02-093, Poland, and ††Department of Biology, University of Iowa, Iowa 52242

ORCID IDs: 0000-0002-0338-4252 (Y.-Y.J.); 0000-0003-3185-7923 (E.J.); 0000-0002-4412-4916 (Z.R.); 0000-0003-4420-4630 (J.G.)

ABSTRACT In a single cell, ciliates maintain a complex pattern of cortical organelles that are arranged along the anteroposterior and circumferential axes. The underlying molecular mechanisms of intracellular pattern formation in ciliates are largely unknown. Ciliates divide by tandem duplication, a process that remodels the parental cell into two daughters aligned head-to-tail. In the *elo1-1* mutant of *Tetrahymena thermophila*, the segmentation boundary/division plane forms too close to the posterior end of the parental cell, producing a large anterior and a small posterior daughter cell, respectively. We show that *ELO1* encodes a Lats/NDR kinase that marks the posterior segment of the cell cortex, where the division plane does not form in the wild-type. Elo1 acts independently of Cdal, a Hippo/Mst kinase that marks the anterior half of the parental cell, and whose loss shifts the division plane anteriorly. We propose that, in *Tetrahymena*, two antagonistic Hippo circuits focus the segmentation boundary/division plane at the equatorial position, by excluding divisional morphogenesis from the cortical areas that are too close to cell ends.

KEYWORDS Lats; Tetrahymena; pattern; ciliate; polarity

CILIATES are among the most sophisticated cell types known. In a single large and polarized cell, ciliates assemble an amazingly complex set of cytoskeletal organelles that are anchored to the plasma membrane at specific positions along the anteroposterior and circumferential axes. The cell cortex—the outermost layer of the cytoplasm which is rich in cytoskeletal structures—is the likely carrier of positional information. For example, *Stentor*, a large ciliate that is amenable to microsurgery, can regenerate its cortical pattern after most of its endoplasm is removed. Furthermore, an endoplasmic mass can regenerate the entire pattern only if at least a small patch of cell cortex is left on the cell surface (Tartar 1956, 1961). The mechanisms that govern the formation, duplication, and regeneration of the cortical pattern in ciliates remain largely unknown, especially at the molecular level. Insights into the pattern formation in ciliates could uncover broader principles of how organelles are positioned inside the cell (Frankel 1989; Kirschner *et al.* 2000; Marshall 2011).

As compared to *Stentor*, *Tetrahymena thermophila* is a much smaller ciliate, which, however, can be studied by forward and reverse genetic approaches (reviewed in Ruehle *et al.* 2016). The main constituents of the cell cortex of *Tetrahymena* are ~20 longitudinal rows of locomotory cilia (reviewed in Wloga and Frankel 2012). A single oral apparatus is located near the anterior cell end, while the contractile vacuole pores (CVPs) and the cytoproct (site of defecation) are positioned at different circumferential positions near the posterior cell end (Figure 1A).

doi: https://doi.org/10.1534/genetics.118.301889
Manuscript received June 29, 2018; accepted for publication December 21, 2018; published Early Online December 27, 2018.
Supplemental material available at Figshare: https://doi.org/10.6084/m9.figshare.7525193.
[1]These authors contributed equally to this work.
[2]Corresponding author: Department of Cellular Biology, University of Georgia, 724 Biological Sciences Bldg., Athens, GA 30602. E-mail: jgaertig@uga.edu

Ciliates divide by "tandem duplication," a process of segmentation that reorganizes the parental cell into two daughters, which emerge aligned head to tail. The segmentation boundary that later becomes the fission line (we will refer to the positions of both structures collectively as the "division plane") must develop at the proper latitude, to produce daughters of equal size, and its positioning operates in the context of the existing pattern of the parental cell.

Several studies have linked the Hippo kinase cascade to tandem duplication in ciliates, and specifically to the division plane positioning (Tavares *et al.* 2012; Slabodnick *et al.* 2014; Jiang *et al.* 2017). The Hippo kinase cascade is a highly conserved eukaryotic signaling pathway that generates diverse outcomes that regulate the animal organ size, cell proliferation, cell growth, cell cycle, cell fate determination, and mechanosensation. The conserved part of Hippo signaling consists of a triad of proteins: an upstream kinase Hippo/Mst, a downstream kinase Lats/NDR, and its activator/adapter Mob (reviewed in Yu *et al.* 2015). In *Tetrahymena*, a knockdown of an ortholog of Mob, Mob1, results in an excessively anterior division plane, and defects in segregation of nuclei and cytokinesis (Tavares *et al.* 2012). We recently showed that an identical phenotype is produced by a loss-of function of CdaI, an ortholog of Hippo/Mst kinases (Jiang *et al.* 2017).

Here we investigate *elo1-1*, a recessive loss-of-function mutation in *Tetrahymena* that results in an opposite phenotype: the division plane forms too close to the posterior cell end (Frankel 2008). Surprisingly, we find that the *ELO1* gene encodes an ortholog of another conserved Hippo pathway component, a Lats/NDR kinase (Johnston *et al.* 1990; Xu *et al.* 1995; Hergovich 2013). Thus, in *Tetrahymena*, deficiencies in different core Hippo signaling proteins result in division plane displacements in opposite directions. While the effects of Elo1 and CdaI are antagonistic, our observations indicate that these proteins operate in two consecutive Hippo signaling circuits. Both proteins occupy cortical areas in which the divisional activities do not occur in the wild type. This and our earlier work (Jiang *et al.* 2017) reveal that cortical inhibition drives intracellular patterning in ciliates.

Materials and Methods

Tetrahymena strains

The *T. thermophila* strain IA388 *elo1-1/elo1-1* (*elo1-1*, mt I) is homozygous for *elo1-1*, a mutation that shifts the division plane toward the posterior cell end (Frankel 2008). Strain IA237 *cdaI-1/cdaI-1* (*cdaI-1*, mt II) is homozygous for *cdaI-1*, a temperature-sensitive mutation that shifts the division plane toward the anterior cell end (Frankel 2008). Strain CU427 *chx1-1/chx1-1* (*CHX1*, cy-s, mt VI) was used for outcrosses and strain B*VII (cy-s, mt VII) was used for self-crosses by "short circuit genomic exclusion" (SCGE) (Bruns *et al.* 1976). Strain CU428 *mpr1-1/mpr1-1* (*MPR1*, mp-s, mt VII) served as the wild type in phenotypic comparisons. All strains were obtained from the *Tetrahymena* Stock Center (Cornell University, Ithaca, NY). Cultures were grown in SPP medium (Gorovsky 1973) with antibiotics (SPPA, Gaertig *et al.* 2013) at 29 or 39°.

Identification of the elo1-1 causative mutation

We used the "allelic composition contrast analysis (ACCA)" as recently described (Jiang *et al.* 2017). IA388 was crossed to CU427, and a single F1 heterozygote (*elo1-1/ELO1*; *chx1-1/CHX1*) was propagated (for ~8 days) to become sexually mature and sensitive to cycloheximide due to phenotypic assortment (Orias and Flacks 1975). A single F1 subclone was crossed to B*VII to induce SCGE and F2 clones were selected with 15 μg/ml cycloheximide; 31 independent F2 clones with the *elo1-1* phenotype and 31 F2 clones with the wild-type phenotype were combined into separate *elo1-1* and wild-type F2 pools, respectively. The pools were grown overnight, starved for 2 days in 60 mM Tris-HCl pH 7.5 at room temperature and total genomic DNA was extracted using the urea method (Gaertig *et al.* 1994).

The two F2 DNA pools were used to make genomic libraries using Illumina Truseq primer adapters and sequenced on an Illumina HiSeq X instrument, which generated paired-end reads of 150 bp length at ~90× genome coverage. The MiModD suite of tools version 0.1.8 (https://sourceforge.net/projects/mimodd/) was used for ACCA-based variant mapping and identification as follows. For contrast mapping, the sequencing reads were aligned to the micronuclear reference genome (GenBank assembly accession GCA_000261185.1; Hamilton *et al.* 2016) and the aligned reads from both pools were used for joint multi-sample variant calling. The resulting variant call dataset was filtered for sites with ≥50× coverage for each of the two pools. Linkage scores contrasting the allelic composition of the mutant with that of the wild-type pool were computed for each retained variant site and the results plotted against genomic (micronuclear) coordinates. For variant identification, the same sequencing reads were aligned to the macronuclear reference genome (GenBank assembly accession GCA_000189635; (Eisen *et al.* 2006)) and the aligned reads subjected to variant calling as above.

Rescue and overexpression

To rescue the mutant phenotype of *elo1-1*, the predicted coding region of TTHERM_00035550, was placed in the *BTU1* locus (Gaertig *et al.* 1999) under control of the cadmium-inducible MTT1 promoter (Shang *et al.* 2002) in the macronucleus using biolistic transformation and paromomycin selection based on a *neo5* marker (Jiang *et al.* 2017). For overexpression in the wild-type background, the MTT1-GFP-TTHERM_00035550 transgene was integrated into the *BTU1* locus in the CU428 strain. To induce overexpression, cells carrying the MTT1-GFP-TTHERM_00035550 transgene were exposed to cadmium chloride at 2.5 μg/ml for 3 hr.

Imaging by microscopy

To study the localization of the Elo1 protein under conditions of expression that are close to native, we attached a sequence encoding GFP to the 3′ end of the TTHERM_00035550 open reading frame (Stover *et al.* 2006) with a linked *neo5*. The tag was introduced into either the wild-type or *elo1-1* background. In the *elo1-1* cells, this led to expression of the Elo1-GFP mutant (G249V) protein. The transgene copy number was increased through phenotypic assortment, by growing transformant clones at increasing concentrations of paromomycin. The construction of the strain that expresses CdaI-GFP at the native locus was described (Jiang *et al.* 2017). The same targeting plasmid was used to make an *elo1-1* strain that expresses CdaI-GFP.

Cells were analyzed by immunofluorescence (Gaertig *et al.* 2013) using the monoclonal anti-centrin 20H5 (EMD Milipore) and polyclonal anti-GFP (Rockland) antibodies, followed by secondary antibodies labeled with either CY3 or fluorescein (Rockland); DNA was stained with DAPI. The images were collected either on a Zeiss LSM 880 confocal microscope or a Zeiss ELYRA super resolution structured illumination (SR-SIM) microscope. The lengths of the emerging daughter cells were measured on the confocal images using NIH ImageJ (Schneider *et al.* 2012). The position of the division plane was quantified as the ratio of the length of the presumptive anterior daughter to the length of the presumptive posterior daughter (A/P ratio). The boundary between the daughters was either the plane of cortical subdivision or (in the early dividers) the plane immediately above the young oral primordium.

Structural analyses of Elo1 protein

The amino acid sequences of *T. thermophila* Elo1 (UniprotID: Q22MG5) and human Lats1 (UniprotID: O95835) were aligned using the default settings of MAFFT v7.058b (Katoh *et al.* 2002). A fragment of human Lats1 (residues 635–697) is present in the structure of Lats1-Mob1complex (PDBID: 5BRK) (Ni *et al.* 2015). Residues in Lats1 that are within 4 Å away from Mob1 were identified using PyMOL 1.7.6 (Grell *et al.* 2006). A homology-based model of Elo1 kinase domain was built using MODELER with the A chain of PDB structure 2F2U as template (Eswar *et al.* 2006; Yamaguchi *et al.* 2006). The G249V point mutation was introduced into the structure using the loopmodel class in MODELER. The models were visualized using PyMOL 1.7.6.

Data availability

Strains and plasmids are available upon request. The authors affirm that all data necessary for confirming the conclusions of the article are present within the article and figures. Supplemental material available at Figshare: https://doi.org/10.6084/m9.figshare.7525193.

Results

The elo1-1 mutation causes the division plane to form at an excessively posterior position

The *T. thermophila elo1-1* mutant clone was isolated in a genetic screen for cortical pattern mutants, following nitrosoguanidine mutagenesis (Frankel 2008). In the wild-type cell, the first sign of cell division is the new oral apparatus (oral primordium) that appears as a group of basal bodies near the right postoral ciliary row at a submedial position (Figure 1A stages 2 and 3, Figure 2A). At the subsequent stage of "cortical subdivision," the ciliary rows become interrupted by gaps aligned around the cell's equator (Figure 1A stage 4, Figure 2B). This is followed by the emergence of new cell ends on the two sides of the cortical subdivision, nuclear divisions and cytokinesis that produce two daughters of about equal size aligned as a tandem (Figure 1A stage 5, Figure 2C).

In the *elo1-1* cells, the oral primordium develops at an excessively posterior (but proper circumferential) position (Figure 2D). Subsequently, the *elo1-1* mutants develop a cortical subdivision too close to the posterior cell end (Figure 2E) and cytokinesis produces a larger anterior and a smaller posterior daughter, respectively (Figure 2F). The position of the division plane was quantified as the ratio of the length of the presumptive anterior daughter to the length of the presumptive posterior daughter (the A/P ratio). The mean value of the A/P ratio was 0.95 ± 0.08 ($n = 27$) in the wild type, consistent with a nearly equal size of the two daughters, and 1.93 ± 0.8 ($n = 23$) in *elo1-1*, indicating that the anterior daughter is about twice the size of the posterior daughter (Figure 2I). Importantly, in *elo1-1*, the A/P ratio decreases as the division progresses (compare Figure 2, D and E and see Figure 5H for further details); despite this partial normalization, invariably the posterior daughter is smaller than the anterior daughter at the end of cytokinesis (Figure 2F). In the wild type, the micronucleus undergoes mitosis at the time of the onset of cortical subdivision (Figure 1A, stages 3–4); in anaphase, the elongated micronucleus is positioned posteriorly to the cortical subdivision (Figure 2B). The wild-type macronucleus undergoes amitosis by constricting at the time of cytokinesis (Figure 1A stages 4–5, Figure 2C). In the *elo1-1* cells, the positions of both the dividing micronucleus and macronucleus were excessively posterior, but in a local agreement with the division plane position (Figure 2, E and F). In ciliates the positions of nuclei in the endoplasm are guided by cues from the cell cortex (Weisz 1951; de Terra 1973, 1975; Cohen and Beisson 1980; Gaertig and Cole 2000). Thus, the cortical guidance of nuclei is unaffected by *elo1-1*. Consequently, each *elo1-1* daughter receives a complete set of nuclei despite the shift in the position of the division plane (Figure 2F). Some *elo1-1* cells have abnormalities in the organization of the longitudinal ciliary rows that can be twisted or abnormally spaced apart (Figure 2, D–F). Overall, the most prominent and earliest defect in the *elo1-1* cells is an excessively posterior initial specification of the division plane.

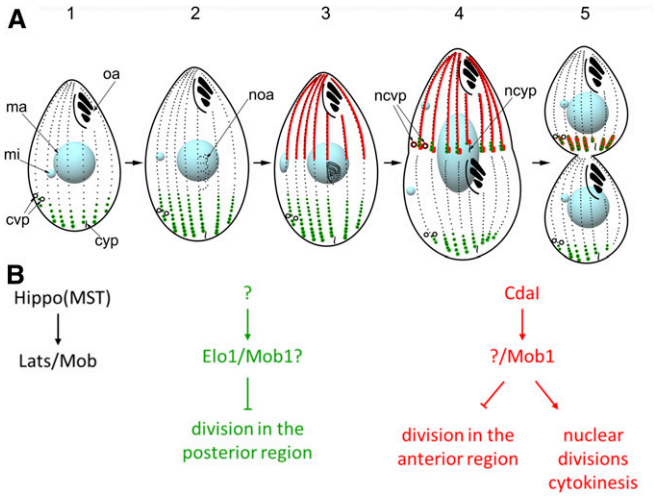

Figure 1 The course of cell division in *Tetrahymena* and its two Hippo signaling circuits. (A) The outline of the stages of cell division in *Tetrahymena*. The localization patterns of Elo1 and Mob1 (green, the two proteins perfectly colocalize) and Cdal (red) are shown. The Mob1 data are based on Tavares *et al.* (2012). The diagram is a modification of the one published in Jiang *et al.* (2017). mi, micronucleus; ma, macronucleus; oa, oral apparatus; noa, new oral apparatus (oral primordium); cvp, contractile vacuole pore; ncvp, new contractile vacuole pore; cyp, cytoproct; ncyp, new cytoproct. The following stages are marked: stage 1, interphase; 2, early oral primordium; 3, late oral primordium; 4, cortical subdivision and mitosis of the micronucleus; 5, cytokinesis and macronuclear amitosis. (B) The proposed composition and the activities of the two consecutive Hippo signaling circuits in *Tetrahymena*. Components of a generic Hippo circuit are shown on the left.

Consequently, all events of cell division occur at excessively posterior positions, but otherwise appear unaffected.

ELO1 encodes a Lats/NDR kinase

We used a comparative whole genome sequencing approach, ACCA (Jiang *et al.* 2017), to map the causal mutation for *elo1-1* (see *Materials and Methods*). Briefly, we prepared pools of either wild-type or *elo1-1* F2 clones (meiotic segregants) derived from a single F1 heterozygote. The pooled genomes were sequenced and the sequence reads were aligned to the micronuclear reference genome (Hamilton *et al.* 2016). For each sequence variant detected, a linkage score was calculated that reflected the degree of cosegregation of the alternate allele with *elo1-1* and the corresponding cosegregation of the reference allele with the wild-type phenotype, respectively. The linkage scores were plotted along the length of the micronuclear chromosomes. This revealed a region of increased variant to phenotype linkage on the micronuclear chromosome 3 between 8 and 9 Mb (Figure 3A). Within this interval, a single sequence variant (a G to T substitution at the micronuclear position chr3:8620427) was supported by 100% alternate allele (T) reads in the pool of 31 mutant F2 clones and 100% reference allele (G) reads in the pool of 31 wild-type F2 clones. In the macronuclear genome, the corresponding base pair position is located in the coding region of *TTHERM_00035550* gene that encodes a protein homologous to the Lats/NDR kinases, conserved components of the Hippo kinase cascade (Hergovich 2013). The predicted amino acid sequence of the conserved portion of TTHERM_00035550 protein that contains the kinase domain (positions 30–475) is 43% identical to the corresponding part of the *Drosophila* Trc (Geng *et al.* 2000), 39% identical to that of CBK1 of the budding yeast (Bidlingmaier *et al.* 2001), and 46% identical to that of the human NDR2 (Millward *et al.* 1995). Reciprocal BLASTp searches using the above mentioned Lats/NDR sequences against the predicted proteome of *T. thermophila* (Eisen *et al.* 2006) returned either TTHERM_00035550 or TTHERM_00283290 (a possible paralog) as top matches. Structural analyses further argue that the TTHERM_00035550 protein is a true Lats/NDR kinase (see below).

The candidate causal mutation produces a G249V substitution. The *elo1-1* allele is recessive (Frankel 2008). To test whether G249V in TTHERM_00035550 is the cause of *elo1-1*, we introduced a transgene expressing a wild-type TTHERM_00035550, as an N-terminal GFP fusion under the cadmium-inducible promoter MTT1 (Shang *et al.* 2002), into the *elo1-1* cells. The dividing *elo1-1* cells with GFP-TTHERM_00035550 had a nearly normal A/P ratio of 0.82 ± 0.12 ($n = 26$) (Figure 2, G–I); this rescue occurred without cadmium ions added, indicating that the basal level of expression under MTT1 was sufficient for complementation of the mutant phenotype. We conclude that the G249V substitution in TTHERM_00035550 is the cause of *elo1-1*, and, therefore, we named the *TTHERM_00035550* gene *ELO1*.

A kinase classification algorithm (Talevich and Kannan 2013; McSkimming *et al.* 2017) confirmed that Elo1 belongs to the Lats/NDR subfamily of the AGC parent group of kinases. Lats/NDR kinases bind Mob—an adapter protein that is a part of the conserved core Hippo pathway (Luca and Winey 1998; Colman-Lerner *et al.* 2001; Weiss *et al.* 2002). An alignment of the amino acid sequences of Elo1 and human Lats1 (Figure 3B) revealed that the two proteins share sequence homology within a region that is N-terminal to the kinase domain, which, in Lats1, serves as a Mob-binding domain (Bothos *et al.* 2005). Several amino acids that, in the human Lats1, lie within 4 Å of the human Mob1 surface (Gógl *et al.* 2015; Ni *et al.* 2015), are conserved at the corresponding positions in Elo1 (blue circles in Figure 3B). Elo1 also has a conserved C-terminal hydrophobic motif (HM) with a threonine (Figure 3B) that, in the Lats/NDR kinases, is phosphorylated by an upstream kinase, Hippo/Mst (Stegert *et al.* 2005). Elo1 also has a serine, S303, in the T loop of the kinase domain (Figure 3B, "P-site"), which is homologous to serines in the well-studied Lats/NDR kinases (*e.g.*, S281 in human NDR1 and S909 in human Lats1) that undergo autophosphorylation, which is required for the kinase activity (Tamaskovic *et al.* 2003; Bichsel *et al.* 2004).

G249 is located within the kinase domain (Figure 3B). To evaluate the impact of G249V, we used homology-based modeling to produce a possible 3D structure of the Elo1 kinase domain (Figure 3C). G249 is located at the beginning of

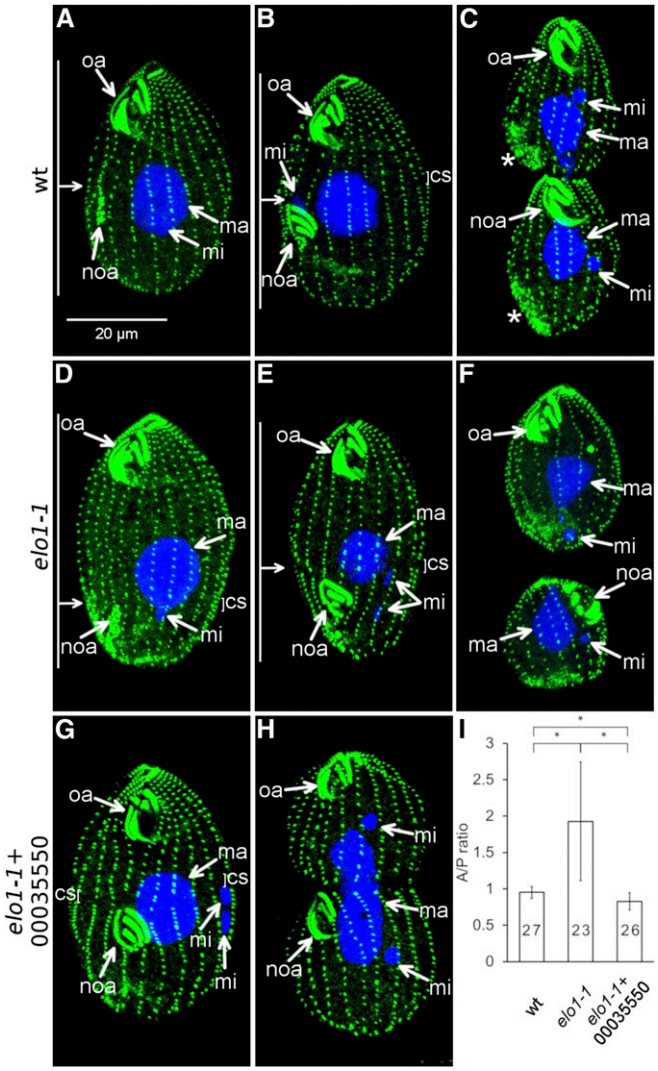

Figure 2 *elo1-1* shifts the division plane to the posterior cell end and expression of a wild-type THERM_00035550 protein rescues this defect. (A–F) The course of cell division in the wild type (A–C) and *elo1-1* (D–F). The cells were labeled with the anti-centrin antibody (green) and DAPI (blue). The anti-centrin labels the basal bodies; in addition in some dividing cells these antibodies mark the vicinity of the contractile vacuoles [stars in (C)]. (A and D) Cells in the earliest stage of cell division (stage 1 in Figure 1A). Note that the oral primordium (noa) is sub-medial in the wild type (A) and excessively posterior in *elo1-1* (D). (B and E) Cells during cortical subdivision (stage 4). (E). The micronucleus (mi) in the *elo1-1* cell (E) is in a more advanced stage of mitosis as compared to the wild-type cell shown in (B). (C and F) Cells undergoing cytokinesis and amitosis of the macronucleus [the *elo1-1* cell shown in (F) is in a more advanced stage]. (G–I) Introduction of a transgene expressing the GFP-TTHERM_00035550 rescues the unequal division in *elo1-1* cells. (G and H) Dividing *elo1-1* cells that carry the MTT1-GFP-THERM_0035550 transgene (grown without added cadmium ions). (I) The graph quantifies the position of the division plane as the ratio of the length of the presumptive anterior daughter to the length of the presumptive posterior daughter (the A/P ratio). Numbers of scored cells are indicated. Error bars are SD and asterisks show significant differences (two-sided *t*-test, $P < 0.01$). oa, oral apparatus; noa, new oral apparatus (primordium); ma, macronucleus; mi, micronucleus; cs, cortical subdivision. On the left side of (A, B, D, and E): the horizontal arrow indicates the position of the division plane and the vertical bars mark the lengths of the presumptive daughter cells.

β8 strand and therefore is not a part of the catalytic center. However, G249 is among the conserved AGC kinase group-specific amino acids (Kannan *et al.* 2007). AGC kinases are regulated by a C-terminal tail domain that is tethered to the kinase domain through a PxxP motif (Kannan *et al.* 2007), which is also conserved in Elo1 (Figure 3C). The 3D model of Elo1 suggests that G249 is in close contact with PxxP (Figure 3C). The PxxP motif is also the binding site for the SH3 domain (Jiang and Qiu 2003). It is possible that G249V alters the release of the C-terminal tail domain (which could affect the kinase activity) or perturbs regulatory interactions between Elo1 and SH3 domain-containing proteins.

Elo1 protein is enriched in the posterior cell cortex where the division plane does not form in the wild type

We added a green fluorescent protein (GFP) to the C-terminal end of Elo1, by engineering the *ELO1* locus. During interphase, Elo1-GFP presented as dots near several most posterior basal bodies in each ciliary row, based on colocalization with centrin (Salisbury *et al.* 1988) (Figure 4, A and A' and Supplemental Material, Figure S1, A–B'). The number of Elo1-GFP-positive basal bodies per row was similar on the ventral and dorsal cell side, indicating that distribution of Elo1 is polarized on the anteroposterior but not on the circumferential axis (Figure S1, A–B'). The posterior cortical zone of Elo1-GFP was present when the oral primordium appeared (Figure 4, B and B'). Along the ciliary row, the intensity of the Elo1-GFP dots decreased gradually toward the cell's anterior end (Figure 4E). Based on the SR-SIM imaging, the most posterior basal bodies of the early oral primordium were located immediately anterior to the edge of the detectable Elo1-GFP (Figure 4F). During cortical subdivision, a new Elo1-GFP zone appeared at the posterior edge of the forming anterior daughter (Figure 4C and Figure S1, C–D'). At the time of cytokinesis, GFP-Elo1 marked the most posterior basal bodies equally strongly in the anterior and posterior daughter (Figure 4D and Figure S1, E–F'). The signal of the mutant protein, Elo1(G249V)-GFP, was weaker as compared to Elo1-GFP, indicating that G249V either decreases the levels of Elo1 or its ability to become enriched at the posterior cortex (the mean pixel intensity of Elo1-GFP over the five most posterior basal bodies was 4.6 times higher in the wild type as compared to *elo1-1*; see Figure S2 for details).

Elo1 (Lats/NDR) and CdaI (Hippo/Mst) act in two consecutive Hippo signaling circuits

In addition to Elo1, the medial position of the division plane depends on CdaI and Mob1, orthologs of the Hippo/Mst kinases and Mob proteins, respectively (Figure 1B). However, a loss of either CdaI or Mob1 moves the division plane closer to the anterior cell end (Tavares *et al.* 2012; Jiang *et al.* 2017). As described above, the effect of Elo1 is apparent at the earliest stage of divisional morphogenesis (the appearance of the oral primordium) (Figure 2). In contrast, in cells expressing a conditional mutant CdaI, the division plane is initially specified correctly and migrates in the anterior

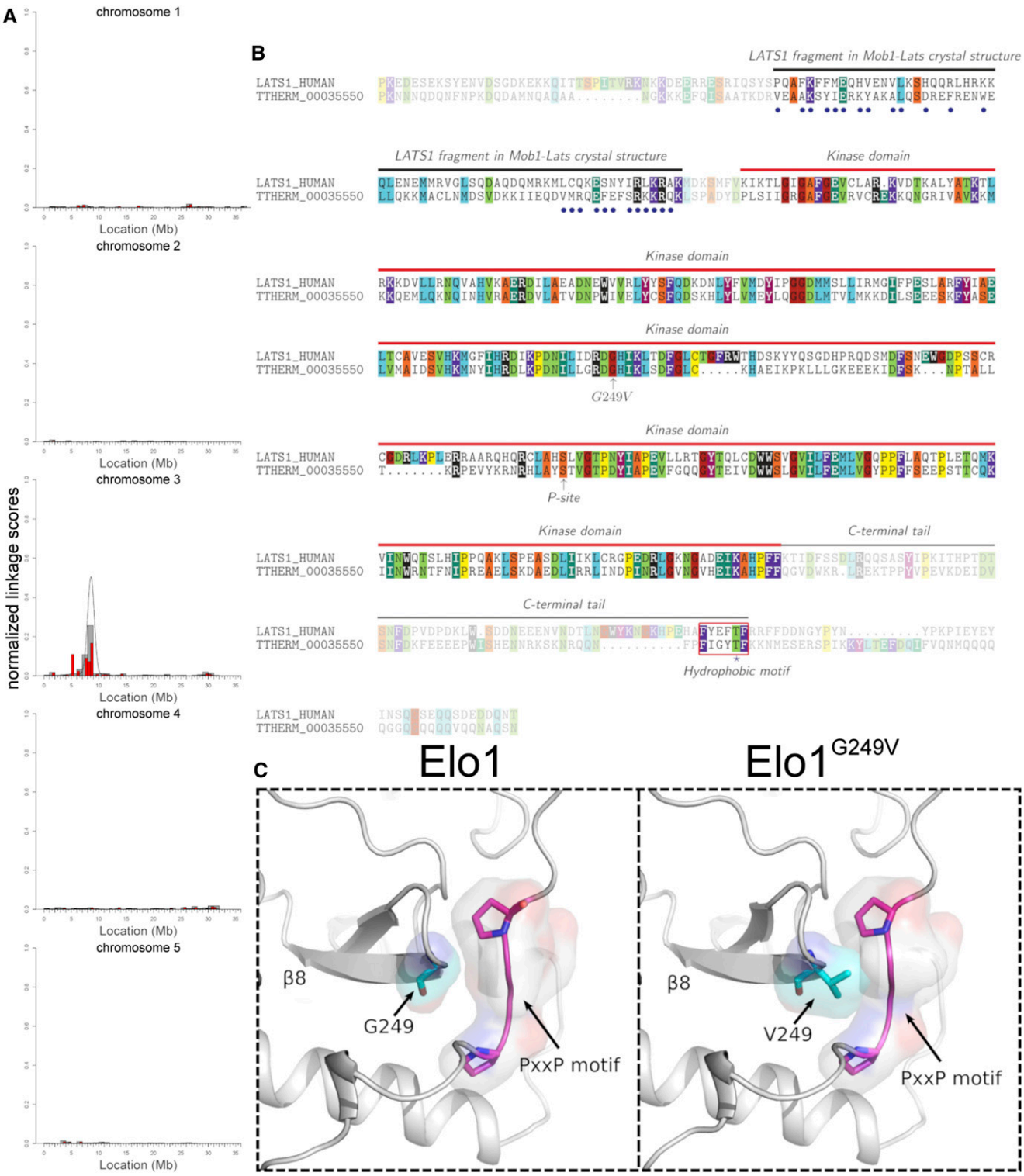

Figure 3 The causal mutation for *elo1-1* is in *THERM_0035550* that encodes a Lats/NDR kinase. (A) The results of mapping of the causal DNA sequence variant for *elo1-1* using ACAA (Jiang *et al.* 2017). Normalized linkage scores are shown along each of the five micronuclear chromosomes. Allelic cosegregation is increased on the left arm of chromosome 3. (B) An alignment of a portion of TTHERM_0035550/Elo1 and human Lats1 amino acid sequences. The blue circles mark the residues that are located within 4 Å from the Mob1 surface in the human Lats1-Mob1 complex (PDBID: 5BRK) (Gogl *et al.* 2015; Ni *et al.* 2015). Different colors represent different sizes of amino acid side chains as follows (in Å^2): dark red, G 88.1; orange, A 118.2, S 129.8; yellow, C 146.1, P 146.8; teal, I 181.0, E 186.2; aqua blue, L 193.1, Q 193.2; H 202.5, M 203.3; violet, F 222.8, K 225.8; purple, Y 238.8; black, R 256.0, W 266.2. The red box highlights the hydrophobic motif (HM). The T-loop serine that undergoes autophosphorylation in the Lats/NDR kinases is marked as the "P-site." (C) The 3D structure of an area of the Elo1 kinase domain showing a fragment of the β8 strand that carries G249 (mutated to V in *elo1-1*). The area is in proximity to the conserved PxxP motif in the C-terminal tail of AGC kinases.

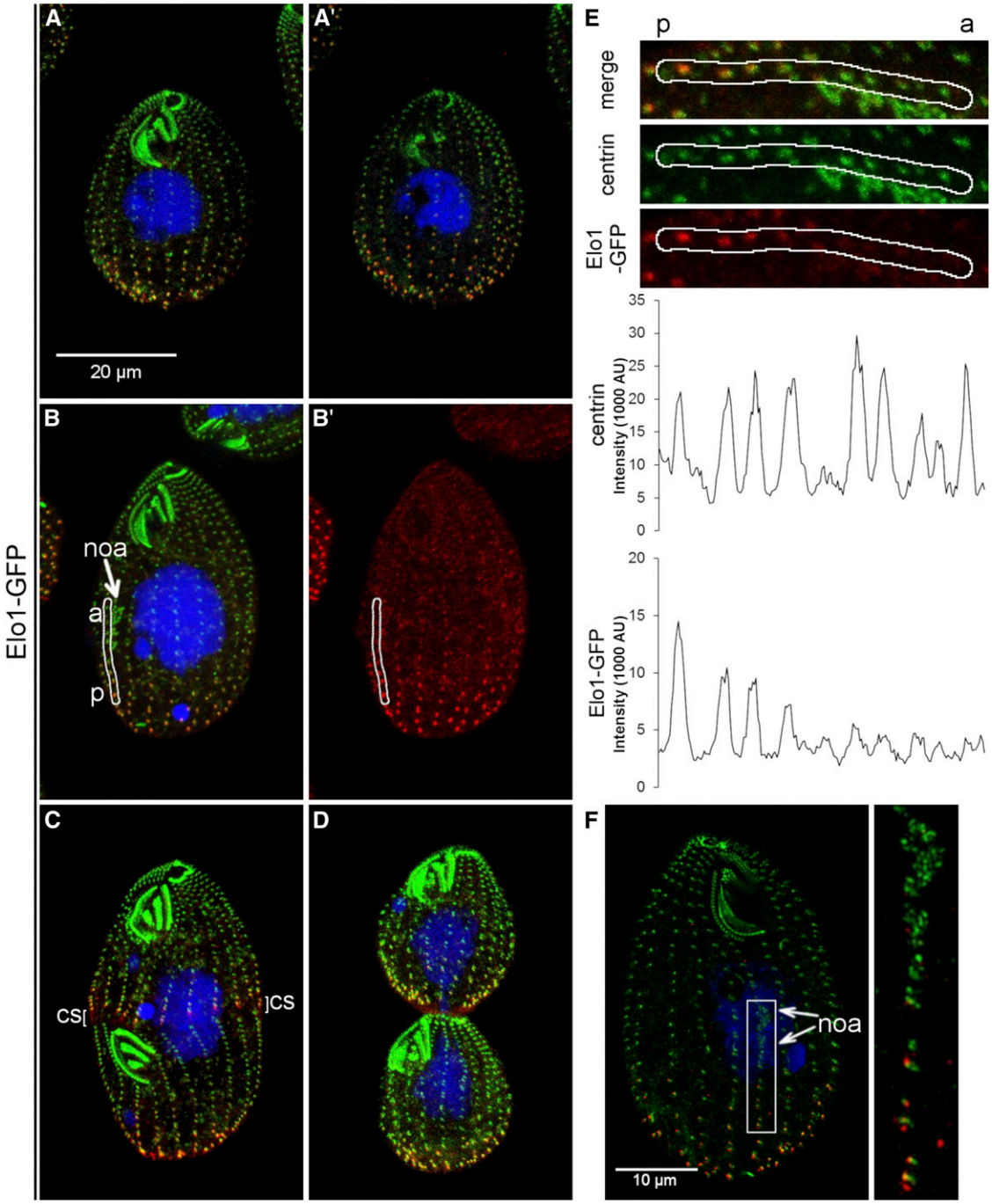

Figure 4 Elo1-GFP is restricted to the posterior cortex. (A–D) Confocal immunofluorescence images of cells expressing Elo1-GFP under the native promoter, labeled with anti-GFP (red), anti-centrin (green) antibodies and DAPI (blue). The cells are in interphase [(A and A′) show the ventral and dorsal side of the same cell, respectively], early cell division with a young oral primordium ((B and B′) show all signals and just Elo1-GFP, respectively), cortical subdivision (C) and cytokinesis (D). (E) Images of a posterior portion of a single ciliary row extracted from the cell shown in (B and B′) (white outline), shown at a higher magnification. The images of Elo1-GFP (red), centrin (green) and both signals are shown. Below are corresponding intensity plots of the Elo1-GFP and centrin signals. Note multiple peaks of Elo1-GFP that correspond to the basal bodies. The signal intensity of Elo1-GFP decreases with the increased distance from the posterior cell end. a, anterior end of the section of ciliary row; p, posterior end of a section of the analyzed ciliary row. (F). An SR-SIM image of a dividing cell labeled with the anti-GFP (red) and anti-centrin (green) antibodies. The cell is in an early stage of development of the oral primordium. Note that the Elo1-GFP signal is visible along each ciliary row from the posterior cell end and to the bottom of the oral primordium. The inset shows a higher magnification of the area where the oral primordium forms. The two arrows mark the anterior and posterior boundaries of the oral primordium where the basal bodies are present on the left side of the stomatogenic ciliary row. noa, new oral apparatus; cs, cortical subdivision.

direction at the onset of cortical subdivision (Jiang *et al.* 2017). These observations suggest that Elo1 and CdaI are parts of two separate Hippo signaling circuits that act at consecutive stages of cell division. To test this idea further, we examined a double mutant. We took advantage of a serendipitous finding that adding GFP to an otherwise wild-type CdaI (*cdaI-gfp* allele) leads to a hypomorphic temperature-sensitive phenotype. At 29° the *cdaI-gfp* cells divide normally (Jiang *et al.* 2017; and Figure 5, A and C). At 39°, the *cdaI-gfp* cells had a mild (but significant) anterior displacement of the division plane (Figure 5, B and C), but lacked nuclear or cytokinesis defects, which frequently occur in the cells expressing the stronger allele, *cdaI-1* (Jiang *et al.* 2017). To determine whether, and when, Elo1 and CdaI interact, we compared the A/P ratios between the *elo1-1* and *elo1-1_cdaI-gfp* cells that were either in the early or late phase of cell division (based on the absence or presence of cortical subdivision, respectively). As already mentioned, in the *elo1-1* single mutants (at both 29 and 39°), the A/P length ratio partially normalized as the division progresses (Figure 2, D and E and Figure 5H). For example, in the *elo1-1* cells (at 39°), the A/P ratio decreased from 2.77 ± 0.7 (n = 14) in the early phase to 1.36 ± 0.12 (n = 15) in the late phase (Figure 5H). In the *elo1-1_cdaI-gfp* double mutant cells examined during the early phase, the A/P ratio was not significantly different from that of the *elo1-1* single mutant cells either at 29 or 39°, indicating that CdaI does not influence the division plane position before the appearance of cortical subdivision (Figure 5, D and H). In the double mutant cells examined during the late phase at 39° (but not at 29°), the division plane significantly shifted anteriorly as compared to *elo1-1* cells alone (Figure 5, E, F, and H). In the late phase at 39°, the A/P ratio was 1.00 ± 0.1 (n = 15) in *elo1-1_cdaI-gfp* as compared to 1.36 ± 0.12 in *elo1-1* (n = 15). To summarize, the double mutant cells initially have the phenotype of *elo1-1* and normalize during the later phase due to the effect of *cdaI*-gfp. Thus, CdaI and Elo1 act antagonistically but affect different stages of cell division (Figure 1B). Elo1 specifies the initial position of the division plane on the anteroposterior axis, while CdaI maintains the equatorial position of the division plane, and, as we showed earlier (Jiang *et al.* 2017), promotes nuclear divisions and cytokinesis.

Overexpression of Elo1 phenocopies a loss of CdaI

To test how important the levels of Elo1 are, we overexpressed GFP-Elo1 (using the cadmium-inducible MTT1 promoter) in a wild-type background. Cells overproducing GFP-Elo1 transgene had a mild anterior shift of the division plane (Figure 6, A and B, cf. Figure 2, A and B). This displacement was apparent already at the stage of early oral primordium (Figure 6A). In these overproducing cells, the GFP-Elo1 zone was greatly expanded to cover almost the entire cell, including the oral primordium and the old oral apparatus (Figure 6, A'–B'). Thus, upon overproduction, the zone of Elo1 expression is larger than what would be expected based solely on the mildly shifted position of the division plane. Likely, another factor limits the ability of Elo1 to mediate the exclusion of the divisional activities from the posterior cortex. The overproduced GFP-Elo1 highlighted the basal bodies, but also the old contractile vacuole pores (Figure 6, A' and B'), suggesting that Elo1 binds to microtubules. We conclude that the size of the cortical domain of the emerging posterior daughter depends on the cellular levels of Elo1.

Next, we examined cells in which the MTT1-GFP-Elo1 transgene operated in the *elo1-1* background. As mentioned earlier, without addition of cadmium ions, most of these cells had a normal equatorial cell division plane (Figure 2, G–I). Unexpectedly, in around one-third of the examined clones with an MTT1-GFP-Elo1 transgene in an *elo1-1* background, induction of overexpression (by cadmium ions for 3 hr) caused a cell cycle arrest, nuclear segregation defects, and a strong anterior displacement of the division plane, which is a phenocopy of the strong *CDAI* loss-of-function allele, *cdaI-1* (Jiang *et al.* 2017); in one clone examined by immunofluorescence, 85% (n = 47) of cells showed a *cdaI-1* phenotype after 3 hr of exposure to cadmium ions (Figure 6, C–D'). Thus, in the *elo1-1* background overproduced GFP-Elo1 could interfere with the function of CdaI. The simplest scenario is that an excessive GFP-Elo1 outcompetes a Lats/NDR kinase that acts downstream of CdaI, for binding to Mob1 (Figure 1B, and see *Discussion*). It remains unclear why this apparent interference with the proposed late Hippo circuit would occur only when GFP-Elo1 is overexpressed in the *elo1-1* background. If the two circuits share the same Mob adapter, Mob1, one possibility is that GFP-Elo1, once loaded onto Mob1 as part of the proposed early Hippo circuit, is less likely than the wild-type Elo1 to be released from the Mob1 complex, to make room for the Lats/NDR kinase that operates in the proposed late Hippo circuit.

Discussion

It is now well established that ciliates utilize the Hippo kinase cascade to execute their unique mode of cell division by tandem duplication [this work and Tavares *et al.* (2012), Slabodnick *et al.* (2014), Jiang *et al.* (2017)]. Tavares and colleagues first linked the Hippo pathway to cell division in ciliates by showing that a knockdown of Mob1 in *Tetrahymena* results in an excessively anterior division plane and defects in cytokinesis and nuclear divisions (Tavares *et al.* 2012). A similar phenotype results from a loss of CdaI, a Hippo/Mst kinase (Jiang *et al.* 2017). Here we find that *ELO1*, whose loss of function displaces the division plane toward the posterior end (Frankel 2008), encodes another Hippo pathway component, a Lats/NDR kinase, a conserved binding partner of Mob adapters. We will argue that the opposite influences of different Hippo pathway proteins on the division plane position reflect the activities of two antagonistic and consecutive Hippo signaling circuits that may share the same Mob adapter, Mob1 (Figure 1B).

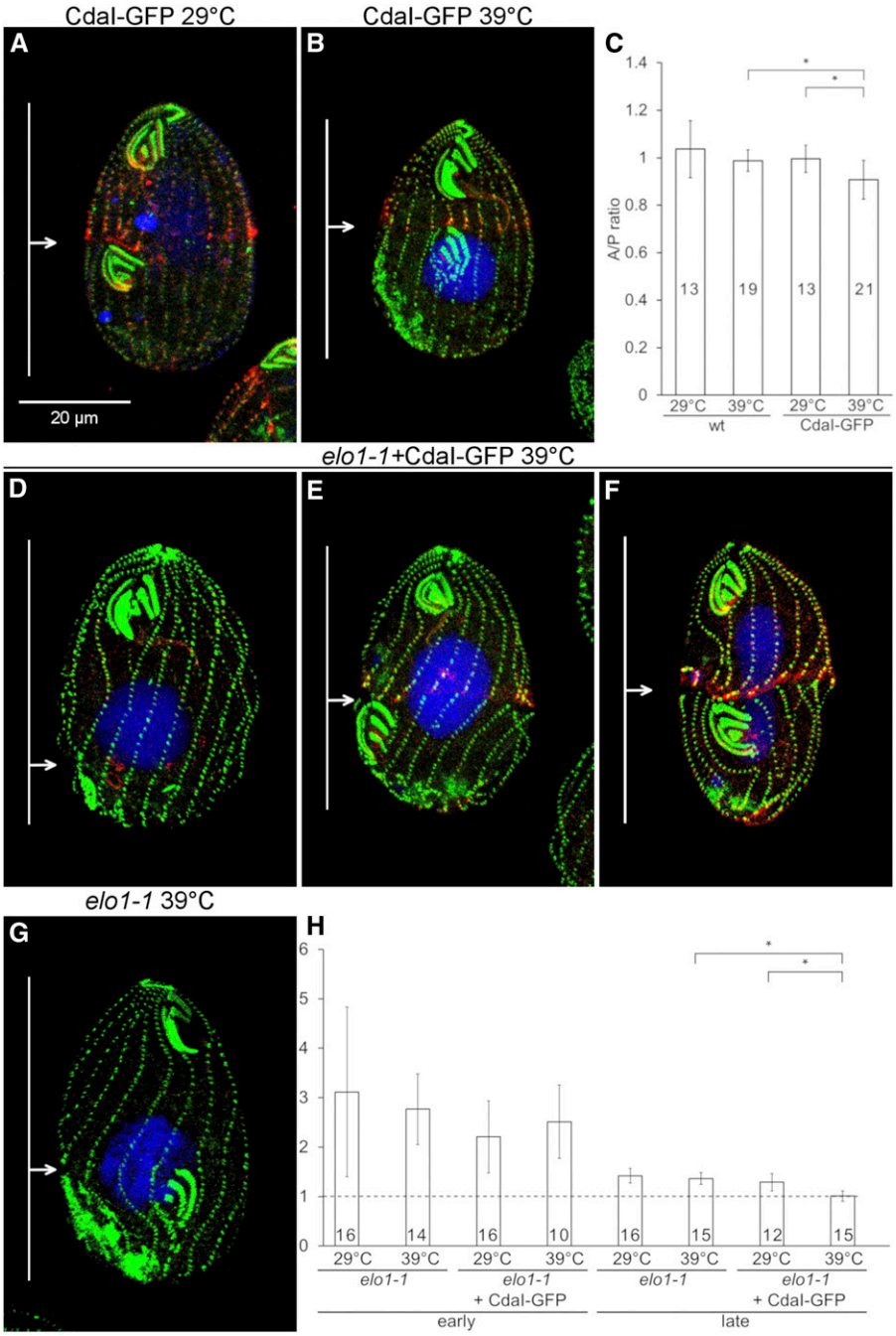

Figure 5 Elo1 and CdaI act in two consecutive Hippo circuits. (A–C) Addition of GFP to the C-terminus of CdaI confers a temperature-sensitive hypomorphic CdaI phenotype (*cdaI-gfp*). The cells are labeled with anti-centrin (green) and anti-GFP antibodies that detect CdaI-GFP (red). (A and B) A *cdaI-gfp* cell at a 29° (A) or 39° (B). Note the anterior shift of the division plane at 39°. (C) The A/P ratios of either wild-type or *cdaI-gfp* cells at 29° or 39° (3 hr exposure). Note a significant decrease in the A/P ratio in the *cdaI-GFP* cells at 39°. Numbers of total scored cells are indicated. Error bars are SD and the asterisks mark significant differences (two-sided *t*-test, $P < 0.01$). (D–F) Double mutant *elo1-1_cdaI-gfp* cells grown at 39°. Note that the division plane is excessively posterior at the earliest stage of cell division (D) and becomes nearly medial in the later stages (E and F). (G) A late phase *elo1-1* cell at 39°. (H) The A/P ratios of *elo1-1* or *elo1-1_cdaI-gfp* cells during either the early or late stage of cell division and either at 29 or 39° (3 hr). The horizontal dotted line represents the A/P ratio value of wild-type cells at 29° at the late phase of cell division. Note the rescue of the A/P ratio in the double mutant at 39°. Numbers of total scored cells are indicated. Error bars are SD and the asterisks mark significant differences (two-sided *t*-test, $P < 0.01$). On the left side of (A, B, and D–G): the horizontal arrow indicates the position of the division plane and the vertical bars mark the lengths of the presumptive daughter cells.

The early Hippo circuit involves Elo1

The *elo1-1* mutation causes the oral primordium to appear at an excessively posterior position. Likely, Elo1 binds to a Mob adapter and acts downstream of an unknown Hippo/Mst kinase (Figure 1B). The Mob partner of Elo1 is likely Mob1, based on the virtually identical localization patterns of the two proteins (Tavares *et al.* 2012 and this study, Figure 1A). However, an inducible knockdown of Mob1 phenocopies a loss of CdaI (Tavares *et al.* 2012; Jiang *et al.* 2017) and not Elo1, consistent with Mob1 acting in the late Hippo circuit (see below). It is therefore possible that Mob1 is shared by the two Hippo circuits. When the depletion of Mob1 is induced in a growing population (Tavares *et al.* 2012), most cells are in interphase and may have a sufficient quantity of Mob1 and Elo1 already loaded onto the posterior cell cortex. Alternatively, Elo1 may bind another Mob adapter. *Tetrahymena* was believed to have only one gene encoding Mob, Mob1 (Tavares *et al.* 2012). However, we note that an unstudied protein TTHERM_001262898 is similar to Mob4, a subtype of Mob present in animal lineages (Trammell *et al.* 2008; Ye *et al.* 2009).

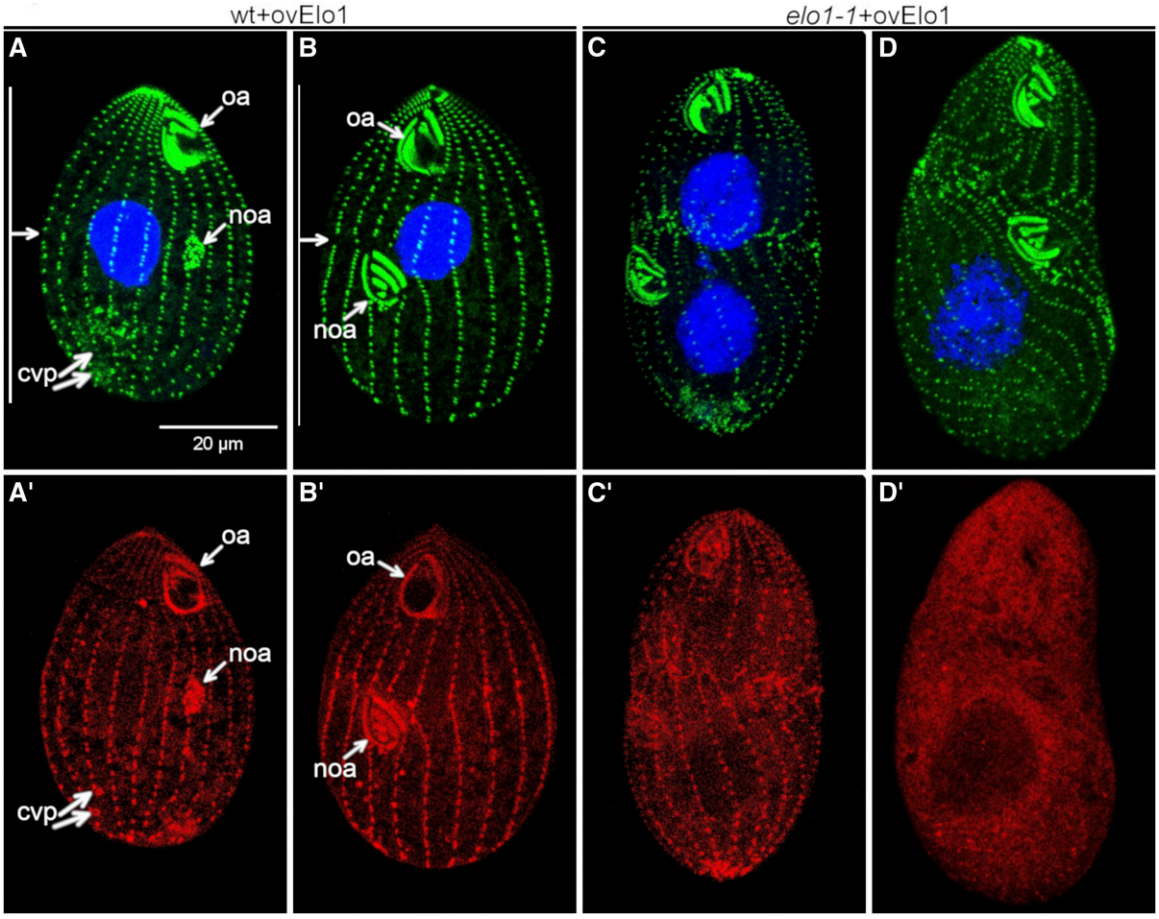

Figure 6 Overexpression of Elo1in the wild-type background shifts the division plane anteriorly, and overexpression in the *elo1-1* background phenocopies a loss of function of CdaI. (A–D′) Images of cells that overproduce GFP-Elo1 in the wild-type (A–B′) or *elo1-1* (C–D′) background (induced by cadmium chloride for 3 hr at 2.5 μg/ml). For each cell the signals of anti-centrin and DAPI (A–D) and anti-GFP-Elo1 (A′–D′) are shown.

CdaI acts in the late Hippo circuit

During expression of conditional alleles of CdaI, the division plane is initially properly positioned (at the stage of oral primordium), and, at the subsequent stage (of cortical subdivision), shifts in an anterior direction (Jiang *et al.* 2017 and this study). This displacement does not appear to be merely a physical process; as the oral primordium moves, the sections of the ciliary rows between the old and new oral apparatus shorten, likely by resorption of their basal bodies (Frankel 2008; Jiang *et al.* 2017). Thus, the division plane migration appears to be a developmental respecification that changes the boundaries of the anterior and posterior daughter. In addition to the control of the division plane position, CdaI is also important for the completion of nuclear divisions and cytokinesis (Jiang *et al.* 2017).

The terminal phenotypes caused by CdaI and Mob1 loss of function are strikingly similar (Tavares *et al.* 2012; Jiang *et al.* 2017), arguing that the late Hippo switch involves CdaI, Mob1, and an unknown Lats/NDR kinase (Figure 1B). While the localization patterns of CdaI and Mob1 are mostly nonoverlapping, the two proteins colocalize at the posterior margin of the forming anterior daughter, and this exact stage of cell division is sensitive to the losses of either CdaI or Mob1 (Tavares *et al.* 2012; Jiang *et al.* 2017).

The unifying property of the two Hippo proteins studied here, Elo1 and CdaI, is that they both act by excluding the divisional activities from parts of the cell cortex. The components of Hippo signaling components studied thus far (Mob1, CdaI, and Elo1) are all asymmetrically localized along the anteroposterior axis, but uniformly distributed along the cell circumference. The unique environment of the cell extremities (such as the different plasma membrane curvatures) could provide cues for the polarization of Hippo proteins. In rod-shaped cells, including fission yeast and bacteria, cell ends are sources of protein gradients that confer spatial control over the cell cycle (reviewed in Kiekebusch and Thanbichler 2014). In the *Tetrahymena con1-1* mutant, an altered shape of the posterior cell end correlates with a posteriorly displaced division plane (Doerder *et al.* 1975; Lynn 1977; Schäfer and Cleffmann 1982). On the other hand, in *Tetrahymena* whose posterior end was destroyed by cell–cell fusion, the oral primordium appears at a correct position and the nuclei are correctly guided with respect to the anteroposterior cell axis (Gaertig and Iftode 1989; Gaertig and Cole 2000). Thus, the

mechanisms that generate the biased cortical localizations of Hippo pathway proteins along the anteroposterior axis remain unknown.

We note that Elo1 and CdaI are not needed for the determination of the different fates of cortical domains that form the daughter cells. Rather, these Hippo proteins regulate the sizes of cortical domains that differentiate into the two daughters. In animals, Hippo signaling regulates the size of body organs by influencing both the rate of cell proliferation as well as the growth rate and ultimately the size of individual cells in the organ (Neto-Silva *et al.* 2010; Tumaneng *et al.* 2012; Lloyd 2013). When Hippo signaling is active, the ciliate is in transition from a single-cell to a transient two-cell stage. Thus, in the broadest terms, the role of Hippo signaling in the control of cell size in a multicellular context might well be conserved between ciliates and animals. Further research of Hippo signaling in the model ciliates has potential for extending our understanding of the mechanisms of pattern formation and the control of cell size.

Acknowledgments

This work was supported by the National Institutes of Health (NIH) grants 1021RR194369 (to J.G.) and 5RO1GM114409 (to N.K.), a bridge funding from the Office of the Vice-President for Research and the Department of Cellular Biology at the University of Georgia (to J.G.), the National Science Foundation grant MCB-1149106 (to N.K.), grants from Deutsche Forschungsgemeinschaft BIOSS CRC746 and CRC850 (to R.B.) and the National Science Centre, Poland Grant 2018/29/B/NZ3/02443 (to E.J.). We thank Muthugapatti K. Kandasamy [Biomedical Microscopy Core facility at University of Georgia, Athens (UGA)] for assistance with fluorescence microscopy.

Literature Cited

Bichsel, S. J., R. Tamaskovic, M. R. Stegert, and B. A. Hemmings, 2004 Mechanism of activation of NDR (nuclear Dbf2-related) protein kinase by the hMOB1 protein. J. Biol. Chem. 279: 35228–35235. https://doi.org/10.1074/jbc.M404542200

Bidlingmaier, S., E. L. Weiss, C. Seidel, D. G. Drubin, and M. Snyder, 2001 The Cbk1p pathway is important for polarized cell growth and cell separation in Saccharomyces cerevisiae. Mol. Cell. Biol. 21: 2449–2462. https://doi.org/10.1128/MCB.21.7.2449-2462.2001

Bothos, J., R. L. Tuttle, M. Ottey, F. C. Luca, and T. D. Halazonetis, 2005 Human LATS1 is a mitotic exit network kinase. Cancer Res. 65: 6568–6575. https://doi.org/10.1158/0008-5472.CAN-05-0862

Bruns, P. J., T. B. Brussard, and A. B. Kavka, 1976 Isolation of homozygous mutants after induced self-fertilization in Tetrahymena. Proc. Natl. Acad. Sci. USA 73: 3243–3247. https://doi.org/10.1073/pnas.73.9.3243

Cohen, J., and J. Beisson, 1980 Genetic analysis of the relationships between the cell surface and the nuclei in Paramecium tetraurella. Genetics 95: 797–818.

Colman-Lerner, A., T. E. Chin, and R. Brent, 2001 Yeast Cbk1 and Mob2 activate daughter-specific genetic programs to induce asymmetric cell fates. Cell 107: 739–750. https://doi.org/10.1016/S0092-8674(01)00596-7

de Terra, N., 1973 Further evidence for cortical control over replication of the macronucleus and basal bodies in Stentor. Dev. Biol. 32: 129–139. https://doi.org/10.1016/0012-1606(73)90225-X

de Terra, N., 1975 Evidence for cell surface control of macronuclear DNA synthesis in Stentor. Nature 258: 300–303. https://doi.org/10.1038/258300a0

Doerder, F. P., J. Frankel, L. M. Jenkins, and L. E. DeBault, 1975 Form and pattern in ciliated protozoa: analysis of a genic mutant with altered cell shape in *Tetrahymena pyriforms* Syngen 1. J. Exp. Zool. 192: 237–258. https://doi.org/10.1002/jez.1401920214

Eisen, J. A., R. S. Coyne, M. Wu, D. Wu, M. Thiagarajan *et al.*, 2006 Macronuclear genome sequence of the ciliate Tetrahymena thermophila, a model eukaryote. PLoS Biol. 4: e286. https://doi.org/10.1371/journal.pbio.0040286

Eswar, N., B. Webb, M. A. Marti-Renom, M. S. Madhusudhan, D. Eramian *et al.*, 2006 Comparative protein structure modeling using Modeller. *Curr. Protoc. Bioinformatics* Chapter 5: Unit-5.6. https://doi.org/10.1002/0471250953.bi0506s15

Frankel, J., 1989 *Pattern Formation. Ciliate Studies and Models*. Oxford University Press, New York.

Frankel, J., 2008 What do genic mutations tell us about the structural patterning of a complex single-celled organism? Eukaryot. Cell 7: 1617–1639. https://doi.org/10.1128/EC.00161-08

Gaertig, J., and E. S. Cole, 2000 The role of cortical geometry in the nuclear development of Tetrahymena thermophila. J. Eukaryot. Microbiol. 47: 590–596. https://doi.org/10.1111/j.1550-7408.2000.tb00095.x

Gaertig, J., and F. Iftode, 1989 Rearrangement of the cytoskeleton and nuclear transfer in Tetrahymena thermophila cells fused by electric field. J. Cell Sci. 93: 691–703.

Gaertig, J., T. H. Thatcher, L. Gu, and M. A. Gorovsky, 1994 Electroporation-mediated replacement of a positively and negatively selectable β-tubulin gene in *Tetrahymena thermophila*. Proc. Natl. Acad. Sci. USA 91: 4549–4553. https://doi.org/10.1073/pnas.91.10.4549

Gaertig, J., Y. Gao, T. Tishgarten, T. G. Clark, and H. W. Dickerson, 1999 Surface display of a parasite antigen in the ciliate Tetrahymena thermophila. Nat. Biotechnol. 17: 462–465. https://doi.org/10.1038/8638

Gaertig, J., D. Wloga, K. K. Vasudevan, M. Guha, and W. L. Dentler, 2013 Discovery and functional evaluation of ciliary proteins in Tetrahymena thermophila. *Methods Enzymol.* 525: 265–284. https://doi.org/10.1016/B978-0-12-397944-5.00013-4

Geng, W., B. He, M. Wang, and P. N. Adler, 2000 The tricornered gene, which is required for the integrity of epidermal cell extensions, encodes the Drosophila nuclear DBF2-related kinase. Genetics 156: 1817–1828.

Gógl, G., K. D. Schneider, B. J. Yeh, N. Alam, A. N. Nguyen Ba *et al.*, 2015 The structure of an NDR/LATS kinase-mob complex reveals a novel kinase-coactivator system and substrate docking mechanism. PLoS Biol. 13: e1002146. https://doi.org/10.1371/journal.pbio.1002146

Gorovsky, M. A., 1973 Macro- and micronuclei of Tetrahymena pyriformis: a model system for studying the structure and function of eukaryotic nuclei. J. Protozool. 20: 19–25. https://onlinelibrary.wiley.com/doi/abs/10.1111/j.1550-7408.1973.tb05995.x

Grell, L., C. Parkin, L. Slatest, and P. A. Craig, 2006 EZ-Viz, a tool for simplifying molecular viewing in PyMOL. Biochem. Mol. Biol. Educ. 34: 402–407. https://doi.org/10.1002/bmb.2006.494034062672

Hamilton, E. P., A. Kapusta, P. E. Huvos, S. L. Bidwell, N. Zafar *et al.*, 2016 Structure of the germline genome of Tetrahymena thermophila and relationship to the massively rearranged somatic genome. eLife 5: e19090. https://doi.org/10.7554/eLife.19090

Hergovich, A., 2013 Regulation and functions of mammalian LATS/NDR kinases: looking beyond canonical Hippo signalling. Cell Biosci. 3: 32. https://doi.org/10.1186/2045-3701-3-32

Jiang, T., and Y. Qiu, 2003 Interaction between Src and a C-terminal proline-rich motif of Akt is required for Akt activation. J. Biol. Chem. 278: 15789–15793. https://doi.org/10.1074/jbc.M212525200

Jiang, Y. Y., W. Maier, R. Baumeister, G. Minevich, E. Joachimiak *et al.*, 2017 The Hippo pathway maintains the equatorial division plane in the ciliate Tetrahymena. Genetics 206: 873–888. https://doi.org/10.1534/genetics.117.200766

Johnston, L. H., S. L. Eberly, J. W. Chapman, H. Araki, and A. Sugino, 1990 The product of the Saccharomyces cerevisiae cell cycle gene DBF2 has homology with protein kinases and is periodically expressed in the cell cycle. Mol. Cell. Biol. 10: 1358–1366. https://doi.org/10.1128/MCB.10.4.1358

Kannan, N., N. Haste, S. S. Taylor, and A. F. Neuwald, 2007 The hallmark of AGC kinase functional divergence is its C-terminal tail, a cis-acting regulatory module. Proc. Natl. Acad. Sci. USA 104: 1272–1277 (corrigenda: Proc. Natl. Acad. Sci. USA 105: 9130 (2008)). https://doi.org/10.1073/pnas.0610251104

Katoh, K., K. Misawa, K. Kuma, and T. Miyata, 2002 MAFFT: a novel method for rapid multiple sequence alignment based on fast Fourier transform. Nucleic Acids Res. 30: 3059–3066. https://doi.org/10.1093/nar/gkf436

Kiekebusch, D., and M. Thanbichler, 2014 Spatiotemporal organization of microbial cells by protein concentration gradients. Trends Microbiol. 22: 65–73. https://doi.org/10.1016/j.tim.2013.11.005

Kirschner, M., J. Gerhart, and T. Mitchison, 2000 Molecular "vitalism". Cell 100: 79–88. https://doi.org/10.1016/S0092-8674(00)81685-2

Lloyd, A. C., 2013 The regulation of cell size. Cell 154: 1194–1205. https://doi.org/10.1016/j.cell.2013.08.053

Luca, F. C., and M. Winey, 1998 MOB1, an essential yeast gene required for completion of mitosis and maintenance of ploidy. Mol. Biol. Cell 9: 29–46. https://doi.org/10.1091/mbc.9.1.29

Lynn, D. H., 1977 Proportional control of organelle position by a mechanism which similarly monitors cell-size of wild-type and conical form-mutant Tetrahymena. J. Embryol. Exp. Morphol. 42: 261–274. http://dev.biologists.org/content/develop/42/1/261.full.pdf

Marshall, W. F., 2011 Origins of cellular geometry. BMC Biol. 9: 57. https://doi.org/10.1186/1741-7007-9-57

McSkimming, D. I., K. Rasheed, and N. Kannan, 2017 Classifying kinase conformations using a machine learning approach. BMC Bioinformatics 18: 86. https://doi.org/10.1186/s12859-017-1506-2

Millward, T., P. Cron, and B. A. Hemmings, 1995 Molecular cloning and characterization of a conserved nuclear serine (threonine) protein kinase. Proc. Natl. Acad. Sci. USA 92: 5022–5026. https://doi.org/10.1073/pnas.92.11.5022

Neto-Silva, R. M., S. de Beco, and L. A. Johnston, 2010 Evidence for a growth-stabilizing regulatory feedback mechanism between Myc and Yorkie, the Drosophila homolog of Yap. Dev. Cell 19: 507–520. https://doi.org/10.1016/j.devcel.2010.09.009

Ni, L., Y. Zheng, M. Hara, D. Pan, and X. Luo, 2015 Structural basis for Mob1-dependent activation of the core Mst-Lats kinase cascade in Hippo signaling. Genes Dev. 29: 1416–1431. https://doi.org/10.1101/gad.264929.115

Orias, E., and M. Flacks, 1975 Macronuclear genetics of *Tetrahymena*. I. Random distribution of macronuclear gene-copies in *T. pyriformis*, syngen 1. Genetics 79: 187–206.

Ruehle, M. D., E. Orias, and C. G. Pearson, 2016 Tetrahymena as a unicellular model eukaryote: genetic and genomic tools. Genetics 203: 649–665. https://doi.org/10.1534/genetics.114.169748

Salisbury, J. L., A. T. Baron, and M. A. Sanders, 1988 The centrin-based cytoskeleton of Chlamydomonas reinhardtii: distribution in interphase and mitotic cells. J. Cell Biol. 107: 635–641. https://doi.org/10.1083/jcb.107.2.635

Schäfer, E., and G. Cleffmann, 1982 Division and growth kinetics of the division mutant conical of Tetrahymena. A contribution to regulation of generation time. Exp. Cell Res. 137: 277–284. https://doi.org/10.1016/0014-4827(82)90028-3

Schneider, C. A., W. S. Rasband, and K. W. Eliceiri, 2012 NIH Image to ImageJ: 25 years of image analysis. Nat. Methods 9: 671–675. https://doi.org/10.1038/nmeth.2089

Shang, Y., X. Song, J. Bowen, R. Corstanje, Y. Gao *et al.*, 2002 A robust inducible-repressible promoter greatly facilitates gene knockouts, conditional expression, and overexpression of homologous and heterologous genes in Tetrahymena thermophila. Proc. Natl. Acad. Sci. USA 99: 3734–3739. https://doi.org/10.1073/pnas.052016199

Slabodnick, M. M., J. G. Ruby, J. G. Dunn, J. L. Feldman, J. L. DeRisi *et al.*, 2014 The kinase regulator Mob1 acts as a patterning protein for Stentor morphogenesis. PLoS Biol. 12: e1001861. https://doi.org/10.1371/journal.pbio.1001861

Stegert, M. R., A. Hergovich, R. Tamaskovic, S. J. Bichsel, and B. A. Hemmings, 2005 Regulation of NDR protein kinase by hydrophobic motif phosphorylation mediated by the mammalian Ste20-like kinase MST3. Mol. Cell. Biol. 25: 11019–11029. https://doi.org/10.1128/MCB.25.24.11019-11029.2005

Stover, N. A., C. J. Krieger, G. Binkley, Q. Dong, D. G. Fisk *et al.*, 2006 Tetrahymena genome database (TGD): a new genomic resource for Tetrahymena thermophila research. Nucleic Acids Res. 34: D500–D503. https://doi.org/10.1093/nar/gkj054

Talevich, E., and N. Kannan, 2013 Structural and evolutionary adaptation of rhoptry kinases and pseudokinases, a family of coccidian virulence factors. BMC Evol. Biol. 13: 117. https://doi.org/10.1186/1471-2148-13-117

Tamaskovic, R., S. J. Bichsel, H. Rogniaux, M. R. Stegert, and B. A. Hemmings, 2003 Mechanism of Ca2+-mediated regulation of NDR protein kinase through autophosphorylation and phosphorylation by an upstream kinase. J. Biol. Chem. 278: 6710–6718. https://doi.org/10.1074/jbc.M210590200

Tartar, V., 1956 Pattern and substance in Stentor, in *Cellular Mechanisms in Differentiation and Growth*, edited by D. Rudnick. Princeton University Press, Princeton, NJ.

Tartar, V., 1961 *The Biology of Stentor*. Pergamon Oress, Elmsford, NY.

Tavares, A., J. Goncalves, C. Florindo, A. A. Tavares, and H. Soares, 2012 Mob1: defining cell polarity for proper cell division. J. Cell Sci. 125: 516–527. https://doi.org/10.1242/jcs.096610

Trammell, M. A., N. M. Mahoney, D. A. Agard, and R. D. Vale, 2008 Mob4 plays a role in spindle focusing in Drosophila S2 cells. J. Cell Sci. 121: 1284–1292. https://doi.org/10.1242/jcs.017210

Tumaneng, K., K. Schlegelmilch, R. C. Russell, D. Yimlamai, H. Basnet *et al.*, 2012 YAP mediates crosstalk between the Hippo and PI(3)K-TOR pathways by suppressing PTEN via miR-29. Nat. Cell Biol. 14: 1322–1329. https://doi.org/10.1038/ncb2615

Weiss, E. L., C. Kurischko, C. Zhang, K. Shokat, D. G. Drubin *et al.*, 2002 The Saccharomyces cerevisiae Mob2p-Cbk1p kinase complex promotes polarized growth and acts with the mitotic exit network to facilitate daughter cell-specific localization of Ace2p transcription factor. J. Cell Biol. 158: 885–900. https://doi.org/10.1083/jcb.200203094

Weisz, P. B., 1951 An experimental analysis of morphogenesis in Stentor coeruleus. J. Exp. Zool. 116: 231–257. https://doi.org/10.1002/jez.1401160203

Wloga, D., and J. Frankel, 2012 From molecules to morphology: cellular organization of Tetrahymena thermophila. Methods Cell Biol. 109: 83–140. https://doi.org/10.1016/B978-0-12-385967-9.00005-0

Xu, T., W. Wang, S. Zhang, R. A. Stewart, and W. Yu, 1995 Identifying tumor suppressors in genetic mosaics: the Drosophila lats gene encodes a putative protein kinase. Development 121: 1053–1063.

Yamaguchi, H., M. Kasa, M. Amano, K. Kaibuchi, and T. Hakoshima, 2006 Molecular mechanism for the regulation of rho-kinase by dimerization and its inhibition by fasudil. Structure 14: 589–600. https://doi.org/10.1016/j.str.2005.11.024

Ye, X., N. Nikolaidis, M. Nei, and Z.-C. Lai, 2009 Evolution of the mob gene family. Open Cell Signal. J. 1: 1–11. https://doi.org/10.2174/1876390100901010001

Yu, F. X., B. Zhao, and K. L. Guan, 2015 Hippo pathway in organ size control, tissue homeostasis, and cancer. Cell 163: 811–828. https://doi.org/10.1016/j.cell.2015.10.044

Communicating editor: A. Gladfelter